AD-A123 065 THE MORPHOLOGY OF A MULTI-BUBBLE SYSTEM IN THE IONOSPHERE(U) NAVAL RESEARCH LAB WASHINGTON DC J CHEN ET AL. 11 JAN 83 NRL-MR-5007 1/1

UNCLASSIFIED F/G 4/1 NL

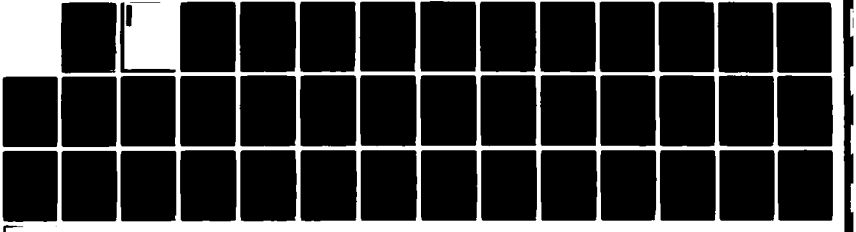

END
DATE FILMED
2 83
DTIC

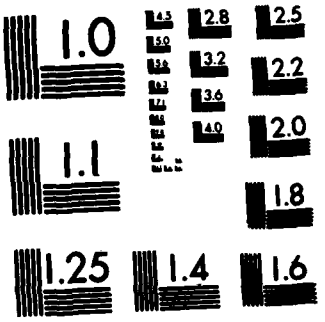

SECURITY CLASSIFICATION OF THIS PAGE (When Data Entered)

REPORT DOCUMENTATION PAGE	READ INSTRUCTIONS BEFORE COMPLETING FORM
1. REPORT NUMBER NRL Memorandum Report 5007	2. GOVT ACCESSION NO. AD-A123065	3. RECIPIENT'S CATALOG NUMBER
4. TITLE (and Subtitle) THE MORPHOLOGY OF A MULTI-BUBBLE SYSTEM IN THE IONOSPHERE	5. TYPE OF REPORT & PERIOD COVERED Interim report on a continuing NRL problem. 6. PERFORMING ORG. REPORT NUMBER
7. AUTHOR(s) J. Chen*, P. Satyanarayana*, and S.L. Ossakow	8. CONTRACT OR GRANT NUMBER(s)
9. PERFORMING ORGANIZATION NAME AND ADDRESS Naval Research Laboratory Washington, DC 20375	10. PROGRAM ELEMENT, PROJECT, TASK AREA & WORK UNIT NUMBERS 61153N; RR033-02-44; 47-0883-0-3; 47-0889-0-3
11. CONTROLLING OFFICE NAME AND ADDRESS Office of Naval Research, Arlington, VA 22217 Defense Nuclear Agency, Washington, DC 20305	12. REPORT DATE January 11, 1983 13. NUMBER OF PAGES 39
14. MONITORING AGENCY NAME & ADDRESS(if different from Controlling Office)	15. SECURITY CLASS. (of this report) UNCLASSIFIED 15a. DECLASSIFICATION DOWNGRADING SCHEDULE
16. DISTRIBUTION STATEMENT (of this Report) Approved for public release; distribution unlimited.	
17. DISTRIBUTION STATEMENT (of the abstract entered in Block 20, if different from Report)	
18. SUPPLEMENTARY NOTES *Present address: Science Applications, Inc., McLean, VA 22102 This research was partially sponsored by the Defense Nuclear Agency under Subtask S99QMXBC, work unit 00067, work unit title "Plasma Structure Evolution," and partially by the Office of Naval Research.	
19. KEY WORDS (Continue on reverse side if necessary and identify by block number) Equatorial Spread F Multi-bubble system Analytic model Rise velocity Striation fingers	
20. ABSTRACT (Continue on reverse side if necessary and identify by block number) A multi-bubble model is developed to study the morphology of a finite array of plasma density depletions (bubbles) in the context of equatorial F-region irregularities during spread F. The Pedersen current conservation equation with quasi-neutrality is solved analytically using an electrostatic analogy. The solution is exact with no *a priori* assumption regarding the separation distance. A two-bubble system with a piecewise constant density profile is first analyzed and the technique is then applied to multi-bubble systems to calculate the polarization electric field and the rise velocities. It is shown that the (Continues)	

DD FORM 1 JAN 73 1473 EDITION OF 1 NOV 65 IS OBSOLETE
S/N 0102-014-6601

SECURITY CLASSIFICATION OF THIS PAGE (When Data Entered)

20. ABSTRACT *(Continued)*

influence of the neighboring bubbles is relatively short-ranged and that a small number of bubbles can adequately model the essential physics in a large array of bubbles. For moderately short separation distances, it is found that the $E \times B$ rise velocity is substantially reduced in comparison with the single-bubble case and that the rise velocity is strongly sheared resulting in the deformation of the contours. The implications of the new morphological results on the stability and dynamical behavior of the bubbles are discussed. The analysis can also be applied to a multi-plasma density enhancement (striation fingers and plasma clouds) system such as one might encounter in plasma cloud striation fingers.

CONTENTS

THE MORPHOLOGY OF A MULTI-BUBBLE SYSTEM IN THE IONOSPHERE

I. INTRODUCTION

The behavior of ionospheric plasma has been extensively studied with the aim of understanding various ionospheric phenomena including equatorial spread F (ESF) and plasma cloud striations (see the following reviews: Ossakow, 1979; Fejer and Kelley, 1980; Ossakow, 1981; Kelley and McClure, 1981; Ossakow et al., 1982). In particular, ESF is thought to be initiated by the Rayleigh-Taylor instability, first proposed by Dungey (1956). In the context of this idea, the plasma density depletions resulting from the instability acquire upward polarization induced $\underline{E} \times \underline{B}$ drift velocities. A large body of literature has since been developed to describe the linear and nonlinear properties of Rayleigh-Taylor plasma density irregularities under various assumptions [Haerendel, 1975; Balsley et al., 1972; Chaturvedi and Kaw, 1975a,b; Hudson and Kennel, 1975.]. In particular, considerable attention has been given to the morphology and motion [Scannapieco and Ossakow, 1976; Ossakow and Chaturvedi, 1978; Ott, 1978; Hudson, 1978; Anderson and Haerendel, 1979; Ossakow et al., 1979; Zalesak and Ossakow, 1980; Zalesak et al., 1982] of plasma depletions ("bubbles") in the equatorial ionosphere. Moreover, a number of observations [Woodman and LaHoz, 1976; Kelley et al., 1976; Hanson and Sanatani, 1971; McClure et al., 1977; Szuszczewicz et al., 1980, 1981] have indicated the presence of rising plasma bubbles.

Another phenomenon of interest is that of the striations in (artificial) plasma "clouds" (density enhancements). This effect has been attributed to the $\underline{E} \times \underline{B}$ gradient drift instability [Linson and Workman, 1970; Volk and Haerendel, 1971] and appears to be amenable to treatments similar to ESF [Scannapieco and Ossakow, 1976; Scannapieco et al., 1976; Ossakow and Chaturvedi, 1978]. The Rayleigh-Taylor instability and the $\underline{E} \times \underline{B}$ gradient drift instability are both interchange modes that may occur in the leading edge of plasma bubbles and backside of clouds respectively. In both cases, the resulting density depletions and enhancements are thought to drift by the polarization induced $\underline{E} \times \underline{B}$ drift. The electric field is produced by the polarization of the plasma across the earth's magnetic field. The essential ingredient is the small but nonzero ion-neutral collision frequency.

Manuscript approved November 24, 1982.

As a result of the initial instability such as the Rayleigh-Taylor instability, an array of density depletions are formed with the wave vector perpendicular to the earth's magnetic field. Moreover, the leading edge of a bubble itself is Rayleigh-Taylor unstable resulting in further "bifurcation" [Ossakow and Chaturvedi, 1978]. Similarly, the $\underline{E} \times \underline{B}$ instability causes the backside of an initial cloud to striate, forming "finger-like" structures. Thus, the plasma depletions and enhancements typically occur in multitudes. Indeed, McClure et al., (1977) and Szuszczewicz et al., (1980;1981) have given evidence for multiple bubbles. In the previous theoretical and numerical simulation works [Ossakow and Chaturvedi, 1978; Anderson and Haerendel, 1979; Zalesak and Ossakow, 1980; Overman et al., 1982], the morphology and evolution have been studied using one-bubble models or a uniformly distributed array of bubbles (clouds). As a result, the intrinsic influence of neighboring bubbles on each other has not been well quantified. Because the bubbles rise due to the polarization induced $\underline{E} \times \underline{B}$ drift, the electric field configuration in and around the bubbles is of central importance.

In the present paper, we study the structure of electrically interacting multi-bubble systems and seek to identify the nature and effects of the mutual interaction. For this purpose, we start with a simple two-bubble configuration in the context of a fluid description and with the emphasis on identifying the basic physics. A simple piecewise constant density profile is used and the electric field inside and outside the bubbles is obtained analytically by the method of images. The method is then applied to multi-bubble configurations. In a sense, the present work is a non-trivial extension of the single bubble work of Ossakow and Chaturvedi (1978).

The scope of the present paper is limited to discussing the morphology of multi-bubble systems and the time-dependent evolution is not explicitly considered. However, the implications of the results will be discussed in the context of the behavior of bubbles consistent with the approximations used in the analysis. Although we primarily discuss the ESF plasma density depletions (bubbles), the technique developed here can be extended straightforwardly to the treatment of plasma density enhancements (clouds).

In Section II, we develop a two-bubble model based on an electrostatic (dielectric) analogy and solve the current conservation equation with quasi-neutrality for the electric field. Section III describes a multi-bubble model and section IV contains the discussion.

II. A TWO-BUBBLE MODEL

A. Formulation

In the present paper, we consider the electric field configuration of electrically interacting multi-bubble systems imbedded in a uniform background plasma and neutral gas. In order to illustrate the basic physics and the theoretical method, we first develop a simple two-bubble model. For his purpose, we adopt a sharp-boundary density profile in which the plasma density is piecewise constant, being uniform inside (n_1) and outside (n_2) the bubbles and having a discontinuity at the bubble boundaries [Haerendel, 1973; Ossakow and Chaturvedi, 1978; Overman et al., 1982]. The bubbles are modelled by two-dimensional cylinders at the same altitude with circular cross-sections and the axis of the cylinders are aligned with the earth's magnetic field which is assumed to be uniform along the positive z-axis. No neutral wind is included. Figure 1 shows schematically the geometry and the coordinate system. The bubbles are located at $x = -x_o$ and $x = x_o$ so that the inter-bubble separation distance is $2x_o$. For reference purposes, we denote the cylinders by C1 and C2, respectively. The radius of each bubble is a. In the equatorial and low latitude regions, the x-axis is along the east-west direction and the gravitational force is along the negative y-axis.

The basic equations in our model are the particle conservation, momentum conservation and current conservation equations [see, for example, Ossakow, 1981]. In addition, quasi-neutrality can generally be assumed on the time scales of interest. In the present paper, we study the morphology of two- and multi-bubble systems by solving the current conservation equation to obtain the instantaneous electric field perpendicular to the magnetic field.

The current conservation equation with quasi-neutrality is

$$\underline{\nabla} \cdot \underline{J} = 0 \tag{1}$$

where $\underline{J}$ is the plasma current density due to ion and electron drifts. Neglecting the inertia terms in the momentum equations for cold ion and electron fluids, the current density in the lab frame can be expressed as (see, for example, Ossakow et al., 1979)

$$\underline{J} = en \left[\frac{1}{\Omega_i} \underline{g} \times \hat{\underline{z}} + \frac{\nu_{in}}{\Omega_i} \left(\frac{1}{\Omega_i} \underline{g} + \frac{c}{B} \underline{E}\right)\right], \tag{2}$$

where $\Omega_i = eB/m_i c$ is the ion cyclotron frequency, $\hat{\underline{z}}$ is the unit vector along the earth's magnetic field, $\underline{g}$ is the gravitational acceleration, n is the plasma density, and ν_{in} is the ion-neutral collision frequency. In (2), we have used the fact that $m_e/m_i \ll 1$ and have neglected the electron $\underline{g} \times \hat{\underline{z}}$ contribution. In addition, in arriving at (2), we have made the approximation $\nu_{in}/\Omega_i \ll 1$. In the F region, ν_{in}/Ω_i is typically of the order of 10^{-2} or less.

The second term in the square brackets in (2) gives the force-field ($\underline{g}$ and $\underline{E}$) aligned drift currents due to the finite ion-neutral collisions. It is convenient to separate the electric field $\underline{E}$ according to

$$\underline{E} \equiv \underline{\tilde{E}} - \frac{m_i}{e} \underline{g}.$$

The term $(-m_i/e)\ \underline{g}$ is the component of $\underline{E}$ cancelling the drift along the gravitational field so that the net drift perpendicular to the magnetic field is described by $\underline{\tilde{E}}$. Then, the current $\underline{J}$ can be written as

$$\underline{J} = \sigma \underline{E}_J \tag{3}$$

where

$$\sigma \equiv \nu_{in} \frac{nec}{B\Omega_i}$$

and

$$\underline{E}_J \equiv \underline{\tilde{E}} + \frac{B}{c\nu_{in}} \underline{g} \times \hat{\underline{z}}. \tag{4}$$

Here, $\underline{B}$ and $\underline{g} = -g\hat{\underline{y}}$ are assumed to be uniform. Physically, $\underline{E}_J$ can be thought of as the electric field driving the current $\underline{J}$ perpendicular to the magnetic field in the frame moving with the velocity $\underline{V}_d = -\Omega_i^{-1}\,\underline{g} \times \hat{\underline{z}}$ relative to the lab frame and σ may be identified as the Pedersen conductivity due to $\nu_{in} \neq 0$.

Equation (1) can now be written in the equivalent form

$$\underline{\nabla} \cdot (n\tilde{\underline{E}}) = -\frac{B}{c\nu_{in}} (\underline{g} \times \hat{\underline{z}}) \cdot \underline{\nabla} n. \tag{5}$$

Perkins et al. (1973) obtained this expression and noted that (5) describes a dielectric immersed in a uniform electric field $\underline{E}_o$ where

$$\underline{E}_o = \frac{B}{c\nu_{in}}\, \underline{g} \times \hat{\underline{z}}. \tag{6}$$

In an earlier work, Longmire (1970) utilized a similar magnetostatic anology to treat the motion of isolated ion clouds. Ossakow and Chaturvedi (1978) used (5) to analytically study a single bubble system. In this dielectric analogy, $\tilde{\underline{E}}$ is the polarization (self) electric field of the bubbles in the uniform field $\underline{E}_o$ and $\underline{E}_J$ corresponds to the total electric field $(\underline{E}_o + \tilde{\underline{E}})$ satisfying the boundary conditions across the bubble boundaries,

$$\begin{aligned} (\sigma \underline{E}_J)_\perp &= \text{continuous} \\ (\underline{E}_J)_\parallel &= \text{continuous} \end{aligned} \tag{7}$$

and at infinity $(x,y \to \infty)$

$$\underline{E}_J \to \underline{E}_o. \tag{8}$$

Note that we have implicitly chosen a reference frame in which the electric field of the distant undisturbed ionosphere is $\underline{E}_o$. The symbols $\parallel$ and $\perp$ refer to the directions parallel and perpendicular to the boundary surfaces, respectively. In the present paper, we also adopt the dielectric analogy and solve the current conservtion equation (1) subject to the above boundary conditions (7) and (8). For this purpose, it is illuminating to

rewrite equation (1) as

$$\underline{\nabla}\cdot(\sigma\underline{E}_J) = 0 \tag{9}$$

In the following section, we describe the method of image dipoles used to solve this "dielectric equation". As a matter of notation, in the remainder of the paper, we use $\underline{E}$ without the subscript J to denote the solution of (9).

B. The Method of Image Dipoles

The problem of solving Poisson's equation (9) with multiple disconnected boundaries is generally difficult. However, in the case treated here with circular cross-sections, the dielectric analogy allows us to construct an exact solution. Consider first a single dielectric cylinder of radius a centered at x = 0 and a line charge density q located at x = b ($|b|>a$). It is well known (Smythe, 1968) that the induced electric field outside the cylinder is that of a line charge $q' = -q(1-K)/(1+K)$ located at $x = a^2/b$ and a line charge $-q'$ located at x=0. The quantity K is the ratio of the dielectric constant (σ_1) inside the cylinder to that outside the cylinder (σ_2)

$$K \equiv \frac{\sigma_1}{\sigma_2} . \tag{10}$$

The induced electric field inside the cylinder is that of a single line charge $q'' = 2q/(1+K)$ located at x = b. If we replace the line charge q by a line dipole moment $\underline{P}_o = P_o\hat{\underline{x}}$ which is equivalent to two equal and opposite line charges separated by a vanishingly small distance, then we find that the electric field due to polarization of the cylinder is that of a single image dipole $\underline{P}$ given by

$$\underline{P} = -\left(\frac{1-K}{1+K}\right)\frac{a^2}{b^2}\underline{P}_o, \tag{11}$$

located at $x = a^2/b$. Note that no image dipole is present on the axis (to be contrasted with the line charge case) and that $\underline{P}_o$ and $\underline{P}$ are colinear, pointing in the opposite directions. The induced electric field inside the cylinder is that due to a dipole moment $\underline{P}^*$ given by

$$\underline{P}^* = \frac{2}{1+K}\,\underline{P}_o \tag{12}$$

located at $x = b$.

We now consider two identical dielectric cylinders of radius a centered at $x = -x_o$ and $x = x_o$ (see figure 1) immersed in a uniform electric field $\underline{E}_o$. Suppose, for the moment, that the two cylinders are non-interacting. Then, for the purpose of calculating the polarization electric field outside the cylinders, each cylinder may be replaced by a dipole moment $\underline{P}_o$ located at $x = -x_o$ and $x = x_o$, where

$$\underline{P}_o = \frac{1}{2}\left(\frac{1-K}{1+K}\right)a^2 E_o\,\hat{\underline{x}}, \tag{13}$$

and K is defined by equation (10). The components of the self electric field are

$$E_x = 2P_o\left[f(x+x_o,y) + f(x-x_o,y)\right], \tag{14}$$

and

$$E_y = 2P_o\left[h(x+x_o,y) + h(x-x_o,y)\right], \tag{15}$$

where

$$f(x,y) \equiv \frac{x^2 - y^2}{(x^2+y^2)^2}, \tag{16}$$

and

$$h(x,y) \equiv \frac{2\,x\,y}{(x^2+y^2)^2}. \tag{17}$$

Here the x- and y-components of the electric field due to a dipole P_o at $x = x_o$ is $2P_o f(x-x_o,y)$ and $2P_o h(x-x_o,y)$, respectively. The electric field $\underline{E}^*$ inside the bubbles is

$$\underline{E}^* = \frac{2}{1+K}\,\underline{E}_o. \tag{18}$$

In the remainder of the paper, asterisks will be used to denote the electric fields inside the bubbles and dipole moments producing the fields.

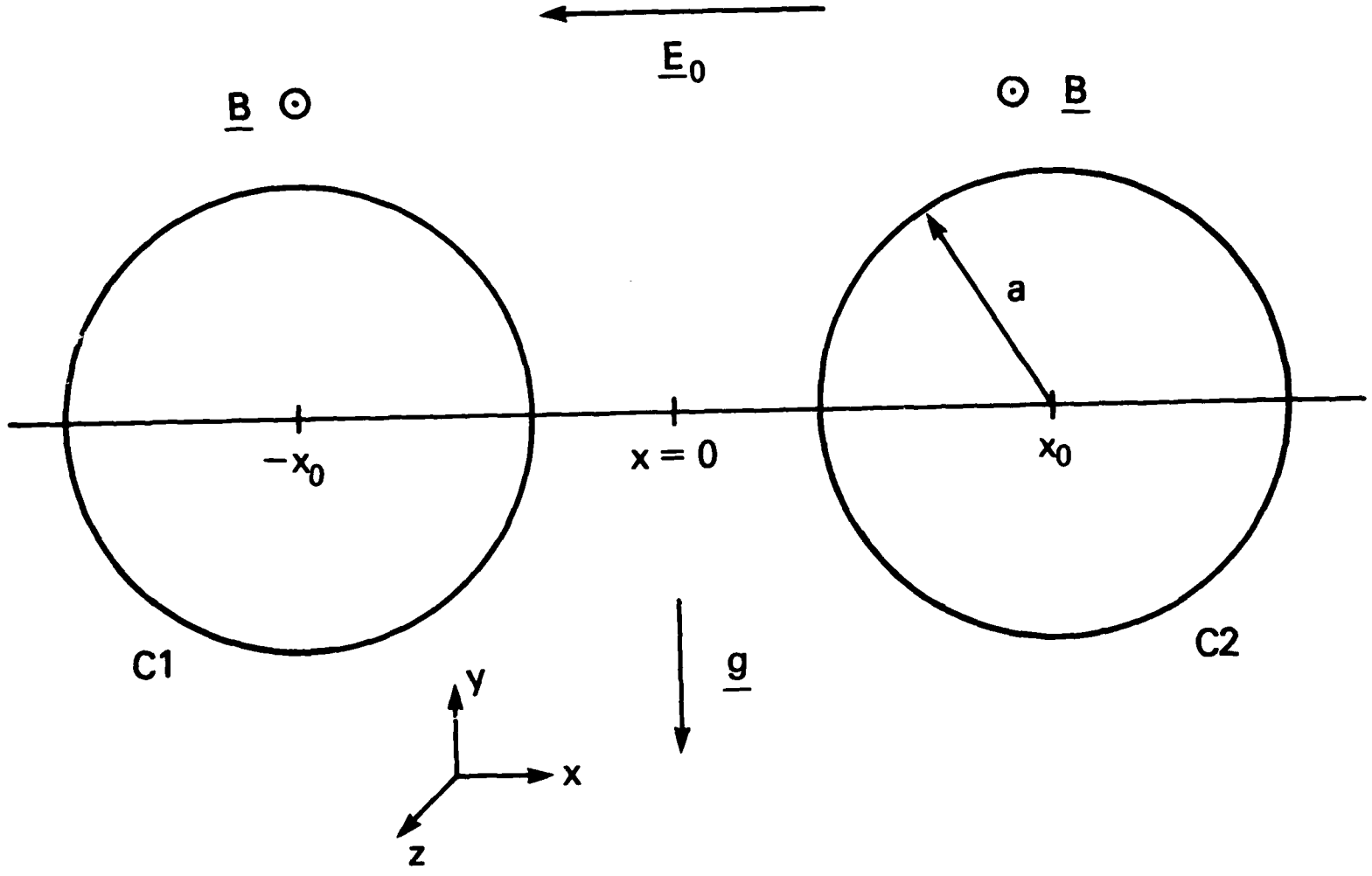

Fig. 1 A schematic drawing of two plasma density depletions and the coordinate system. The depletions have circular cross-sections and are infinite in extent along the z-direction.

We now allow the two cylinders to interact with each other. In addition to the uniform external field $\underline{E}_o$, each cylinder experiences the dipole field of the other. As a result, each cylinder is further polarized giving rise to image dipoles as given by (11) and (12). Iterating the method of image dipoles described above, it is straightforward to show that the total field outside the bubbles is given by

$$E_x = - E_o + \sum_{n=0}^{\infty} 2P_n\left[f(x+x_n,y) + f(x-x_n,y)\right], \tag{19}$$

and

$$E_y = \sum_{n=0}^{\infty} 2P_n\left[h(x+x_n,y) + h(x-x_n,y)\right], \tag{20}$$

where f and h are defined by (16) and (17). Here, for $n \neq 0$,

$$P_n \equiv - \left(\frac{1-K}{1+K}\right) \frac{a^2}{b_n^2} P_{n-1}, \tag{21}$$

$$b_n \equiv x_o + x_{n-1}, \tag{22}$$

and

$$x_n \equiv x_o - \frac{a^2}{x_o+x_{n-1}} \quad . \tag{23}$$

For $n = 0$, we have $x_n = x_o$ and P_o is given by (10).

Similarly, the total electric field inside each cylinder, say, (C2) located at $x = x_o$, is found to be

$$E_x^* = - \frac{2}{1+K} E_o + \frac{2}{1+K} \sum_{n=0}^{\infty} 2P_n f(x+x_n,y), \tag{24}$$

and

$$E_y^* = \frac{2}{1+K} \sum_{n=0}^{\infty} 2P_n h(x+x_n,y) \ , \tag{25}$$

where P_n and x_n are defined above. For the other bubble (C1), the field is obtained by replacing x_o with $-x_o$ in the functions f and h.

It can be seen from (19)-(23) that the convergence properties of these series depend on the parameter s defined by

$$s \equiv \frac{1-K}{1+K} \frac{a^2}{(2x_o)^2} . \tag{26}$$

Each successive line dipole moment is reduced by a factor of s and a geometrical factor of order unity from the preceding one. Since $x_o > a$, we have $|s| < 1/4$ for any K. As a result, the series are generally rapidly convergent except for very small center-to-center separation distances ($x_o \sim a$).

C. Applications

In order to apply the above dielectric results to the ionospheric bubble and cloud problems in accordance with the dielectric analogy (equations (5) and (6)), we identify the dielectric constant σ with the Pedersen conductivity defined in Section II and recall that $\underline{E}_o$ is given by equation (6). Note that the Pedersen conductivity is proportional to the plasma density so that

$$K = \frac{n_1}{n_2} ,$$

where n_1 and n_2 are the plasma densities inside and outside the bubbles. With these identifications, equations (19), (20), (24) and (25) describe the electric field of a two-bubble system in the frame moving with $\underline{V}_d = -\Omega_i^{-1} \underline{g} \times \hat{\underline{z}}$ relative to the earth. Note that our formalism guarantees that the field components obtained above exactly satisfy equation (9) and the boundary conditions (7) and (8), as can be verified easily. Thus, the solution is unique. It is also worth noting that all the image line dipole moments are aligned with the x-axis and no higher multipoles such as quadrupole moment arise. If the bubbles are at different heights, the interaction can still be expressed as a series of image dipole moments that are parallel to the x-axis but the images are not induced on the x-axis itself.

As a result of the polarization electric field, the plasma bubbles (density depletions) $\underline{E} \times \underline{B}$ drift. The drift velocity relative to the distant undisturbed ionosphere where the electric field is $\underline{E}_o$ is given

by $\underline{V} = c\,(\underline{E}^* - \underline{E}_o) \times \underline{B}/B^2$. In particular, the single-bubble rise velocity $\underline{V}_1$ is (using equation 18)

$$\underline{V}_1 = -\left(\frac{1-K}{1+K}\right)\frac{1}{\nu_{in}}\,\underline{g}. \tag{27}$$

For bubbles, $K < 1$ and $\underline{V}_1$ is upward. This result has been obtained by Ossakow and Chaturvedi [1978]. Because $\underline{g}$ is assumed to be uniform, a single isolated bubble maintains its circular cross-section as it rises with the constant velocity $\underline{V}_1$. The presence of a second bubble, however, modifies the rise velocity significantly. In particular, it is no longer uniform and the cross-sections do not remain unchanged. We have numerically carried out the summations indicated in (19), (20), (24), and (25). The results are depicted in figure 2. The solid lines represent the self electric field lines or equivalently the Pedersen current lines while the dashed lines correspond to the instantaneous $\hat{\underline{E}} \times \underline{B}$ drift velocity ($\underline{V}_2$) for a two-bubble system ($2x_o = 2.5a$ and $K = 0$ for 100% depletion). This figure shows only one quadrant; the actual system is spatially uniform in the z-direction and is symmetric about the y-z plane and the x-z plane. The solid electric field lines are such that the line density is proportional to the field strength. This figure clearly shows that the electric field inside the bubble is significantly modified from the uniform field of an isolated bubble (see (18)). As a general remark, the interaction vanishes as $K \to 1$ and the separation distance increases to infinity.

In this example, the electric field strength at the point A ($x = x_o - a$, $y = 0$) is approximately 1/3 of that at B ($x = x_o + a$, $y = 0$). The prominently nonuniform electric field inside the bubbles has a number of important implications for the dynamic behavior of the two-bubble system. The drift lines (dashed) in figure 2 show that different regions of a bubble undergo drift in the east-west ($\hat{\underline{x}}$) direction with respect to the undisturbed ionosphere. This horizontal drift can be a significant fraction of the vertical rise velocity at some points inside the bubble. For example, $|E_y^*/(E_x^* - E_o)| \tilde{=} 0.55$ at $r = a_-$, and $\theta = \pi/8$ where r is the radial distance from $x = x_o$, a_- is just inside the bubble surface and θ is measured from the point A ($\theta = 0$). Here, $x_o = 1.25$ and $K = 0$ have been used (figure 2). The reason for the strong divergence in the field lines

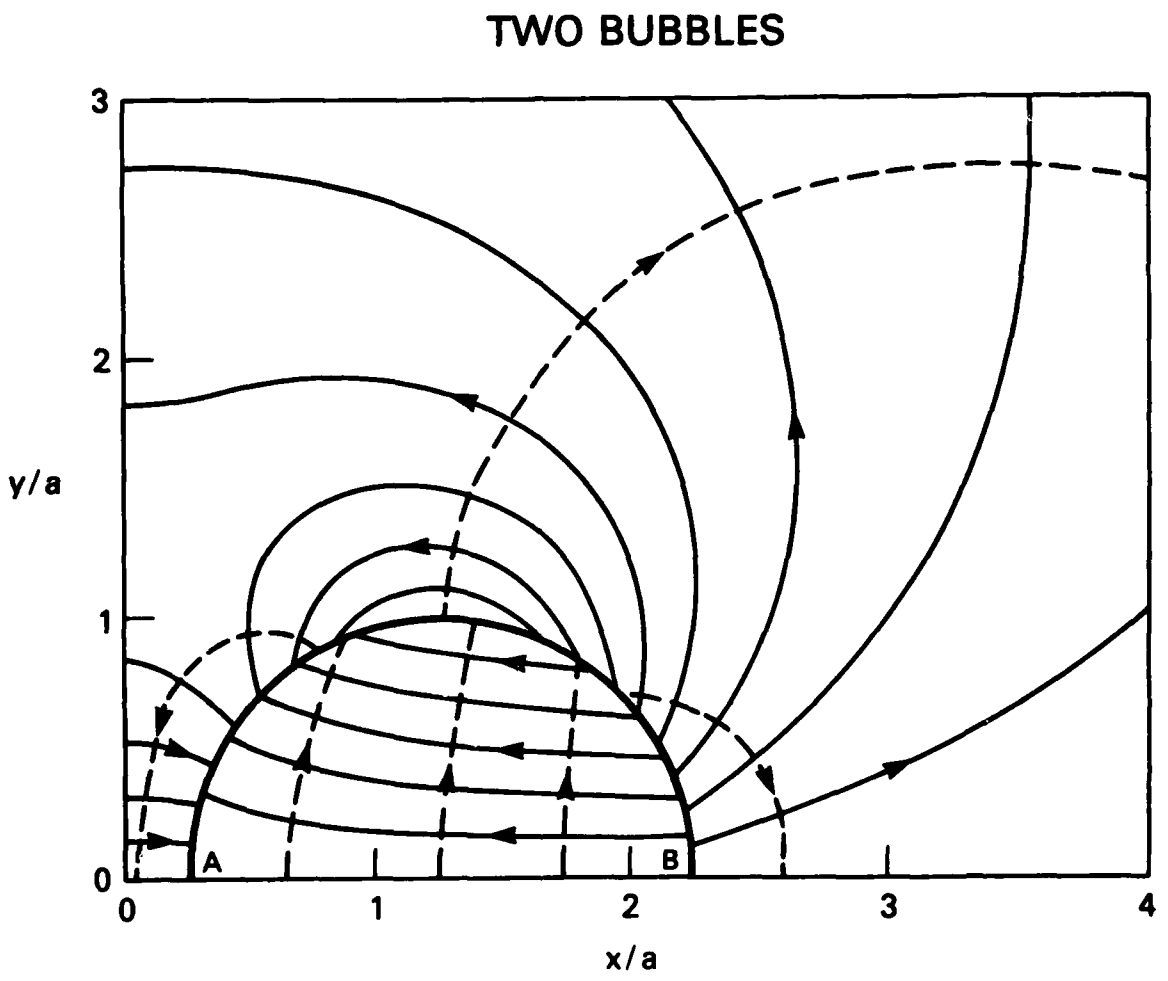

Fig. 2 A drawing of the electric field lines (solid lines) and the $\underline{E} \times \underline{B}$ drift lines (dashed lines) showing one quadrant of a two-bubble system. The system is symmetric about the x-z plane and y-z plane. The separation distance is $2x_o = 2.5a$ and $K = 0$ (100% depletion). The points A and B are inside the bubbles at $x = x_o - a$ and $x = x_o + a$, respectively.

is that the dipole field due to one bubble opposes the internal field of the other bubble.

Figure 3 shows the two-bubble rise velocity (V_y) at a number of points inside the bubble (C2) relative to the uniform rise velocity V_1 of a single bubble given by (27). The ratio $R_2 \equiv V_y/V_1$ is plotted for the interior points A and B (figure 2) as a function of x_o/a. We note that the rise velocity V_y is strongly affected by the neighboring bubble for center-to-center separation distances ($2x_o$) smaller than 5a to 6a. Moreover, comparing V_y at A and at B, we see that the $\underline{E} \times \underline{B}$ drift velocity is sheared. This, together with the conclusions of the preceding paragraph, implies that an initially circular cross-section would not remain circular so that the two-bubble system described here does not correspond to a steady-state system. This should be contrasted with single-bubble models in which steady-state solutions are possible for piecewise constant density profiles. Because a neighboring bubble generally introduces nonuniformity in the electric field, it seems difficult to construct a steady-state two-bubble system unless x_o/a is large.

In interpreting the results, we note that our results do not include the time-dependence. The above field configuration exists if the two-bubble system as described is created at some time (say, $t = 0$). Thus, it would be appropriate as a consistent initial condition for the purpose of studying the subsequent time-evolution. In practice, the drift lines shown in figure 2 are expected to closely approximate the actual evolution for some period of time after $t = 0$ until the distortion changes the field topology significantly. However, the general feature of the field with the weakest x-component and hence the slowest rise velocity in the region nearest to the neighboring bubble should remain unchanged in time.

III. A MULTI-BUBBLE MODEL

In the preceding section, we have discussed in detail a two-bubble model. In considering a multi-bubble system that may be applicable to the ESF phenomenon, the basic physics and the theoretical treatment remain unchanged. However, as the number of bubbles increases, so does the number of image dipoles. For an N-bubble system, the n^{th} order expression must

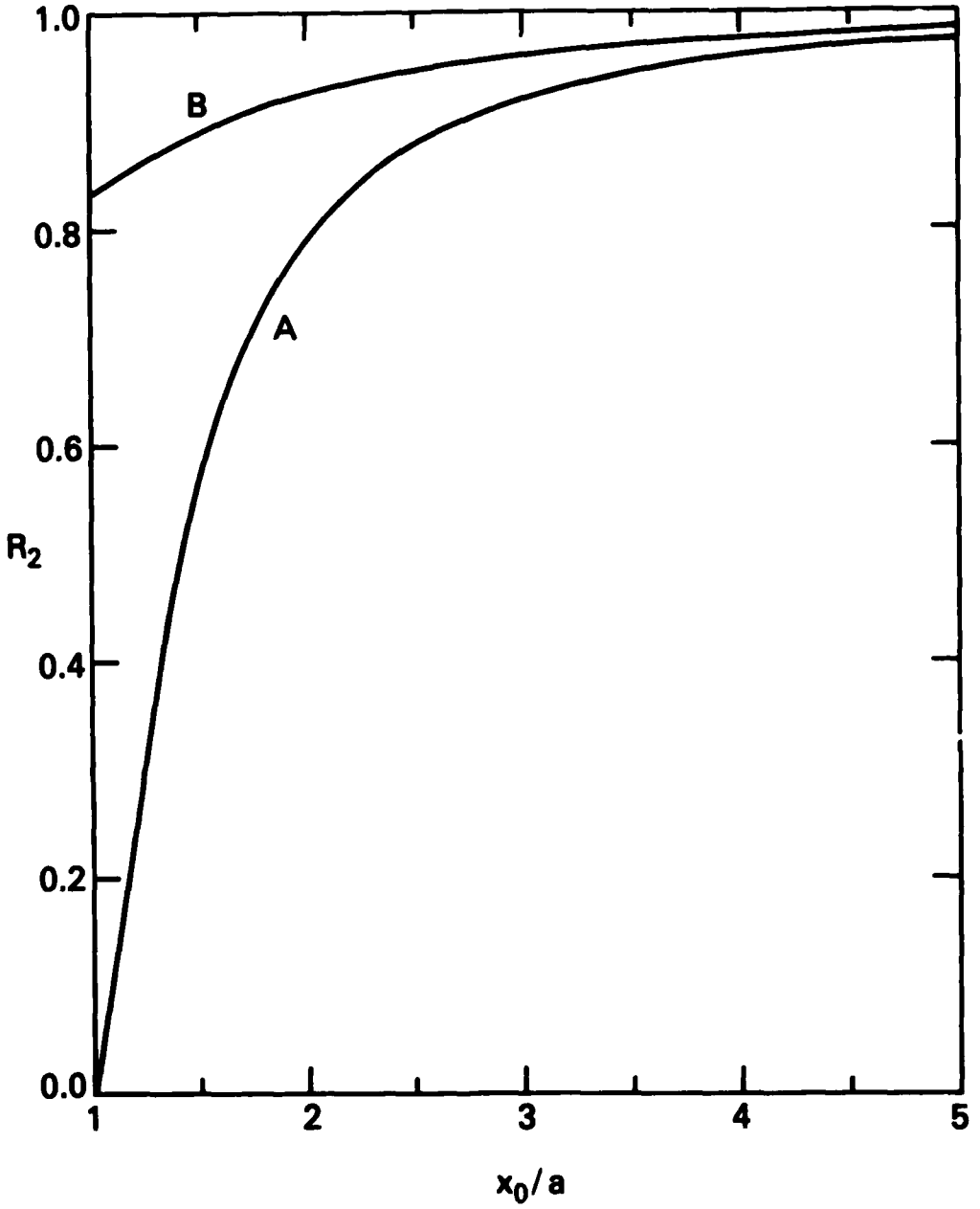

Fig. 3 The ratio R_2 of the vertical rise velocity V_y of a two-bubble system to the single-bubble rise velocity V_1 (equation (27)) as a function of x_o/a. The separation distance is $2x_o = 2.5a$ and $K = 0$ (100% depletion). The curve A corresponds to the point A ($x = x_o - a$) and the curve B to the point B($x = x_o + a$) in figure 2.

include $N(N-1)^n$ image dipoles. Fortunately, the influence of a bubble decreases as the inverse square of the separation distance. Thus, the nearest and the second nearest neighbors are expected to have the dominant effects. A consideration of equations (11) and (12) shows that the second nearest neighbors have effects of the order of $4^{-2}E_o \approx 0.06\ E_o$ and that the third nearest neighbors have effects of the order of $6^{-2}E_o \approx 0.03\ E_o$ for a given value of $a/x_o < 1$. This means that the inter-bubble (and also inter-cloud) interaction is short-ranged and that the third nearest neighbors and beyond have no significant influence. Thus, only a small number of bubbles are necessary to model an N-bubble system with $N \gg 1$. Note that the influence of the bubbles still vanishes at infinity, differing from systems satisfying periodic boundary conditions.

The theoretical treatment described is exactly applicable to any N. However, in the remainder of this section, we include up to a total of 5 mutually interacting bubbles. The mathematical manipulations involved are analogous to those of the preceding section, resulting in series expressions similar to (19), (20), (24), and (25). As before, only dipole moments, not higher multipoles, are induced. Since no new insight is to be gained by examining the actual expressions, we give below only the results. In figure 4, we show the electric field and drift configurations of a system with three plasma depletions. The three depletions are again modelled by cylinders of radius a, located at $x = -2x_o$, 0, and $2x_o$. Only one quadrant is shown. The neighboring bubbles are separated by a distance $2x_o = 2.5a$, and are 100% depleted ($K = 0$) as before. The "external" electric field is $\underline{E}_o$ given by (6), and the density profile is piecewise constant. The solid lines represent the polarization electric field without $\underline{E}_o$. The quantity $c\,(\underline{E}^* - \underline{E}_o) \times \underline{B}\,/B^2$ is then the instantaneous drift velocity relative to the distant undisturbed ionosphere and is represented by the dashed lines. Although the three-bubble system is different from a two-bubble system in that the former has a central bubble about which the system is symmetric, the general features of the field and drift configurations are similar as can be seen by comparing figures 2 and 4. That is, the field lines and drift lines inside and around the end bubbles of the three-bubble system (figure 4) are similar to those of the two-bubble system (figure 2) because the dominant influence arises from the nearest neighbors. The central bubble in the three-bubble

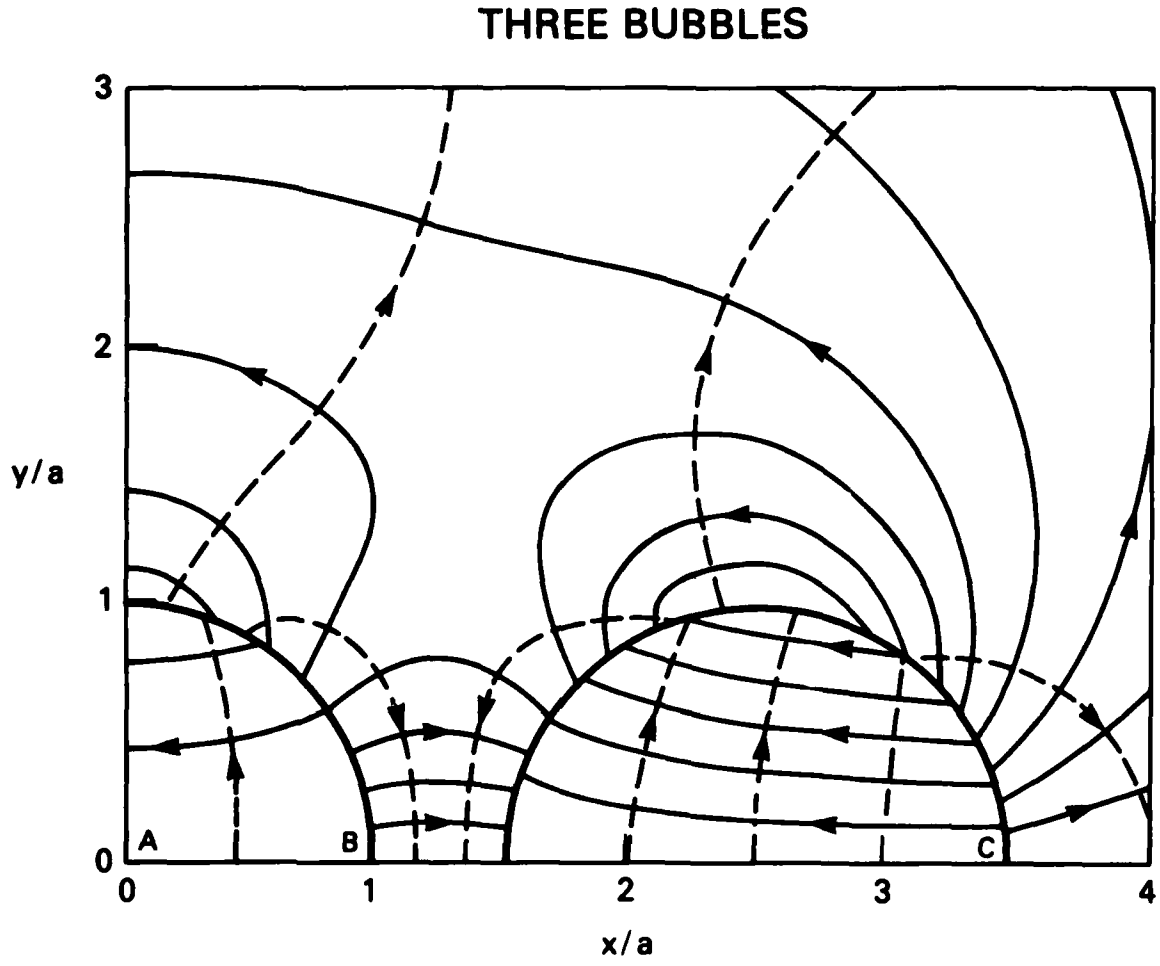

Fig. 4 A drawing of the electric field lines (solid) and the $\underline{E} \times \underline{B}$ drift lines (dashed), showing one quadrant of a three-bubble system. The bubbles are placed at $x = \pm 2x_o$ and $x = 0$. The points A, B, and C are inside the bubbles at $x = 0$, $x = a$, and $x = 2x_o + a$. The separation distance is $2x_o = 2.5a$ and $K = 0$ (100% depletion).

system is affected by two neighboring bubbles with comparable effects. The field is markedly reduced in the region nearest a neighboring bubble (point B in figure 4).

Figure 4 also shows the distortion in the electric field which renders the system non-steady-state, as in the two-bubble case. The drift velocity (dashed lines) has an east-west (horizontal) component that may be a significant fraction of the vertical velocity. For example, $|E_y^*/(E_x^*-E_o)| \tilde{=} 0.48$ at $\theta = \pi/8$ from the point B just inside the boundary of the central bubble and $|E_y^*/(E_x^*-E_o)| \tilde{=} 0.55$ at $\theta = \pi/8$ from the point $x = x_o-a$ and $y = 0$ just inside the boundary of the side bubble. Thus, in the neighborhood of these points, the bubble elements should have significant horizontal drifts.

In addition to the distortion of bubble contours resulting from the non-uniform electric field, the figure also shows that the electric field is substantially reduced from that of an isolated single bubble. This fact is illustrated in figure 5 which gives $R_3 \equiv |V_y/V_1|$ for the points A, B and C corresponding to $x = 0$, $x = a$ and $x = 2x_o + a$, all just inside the bubble surfaces. Here, V_y is the vertical drift velocity of the three-bubble system relative to the distant ionosphere. Comparing figure 5 with figure 3, we note that the qualitative behaviour of the rise velocity is similar in both systems, exhibiting significant reduction from that of a single bubble system. However, in the three bubble configuration, the electric field inside the central bubble is substantially weaker than the two neighboring bubbles. Thus, the central bubble has the slowest rise velocity. The line D in figure 5 gives the relative vertical rise velocity of a five-bubble system calculated at $x = a_-$. Curve D, to be compared with curve B, shows that the influence of the additional bubble on the field inside the central bubble is small. The reduction in rise velocities is increased as the number of bubbles is increased. However, the influence of the bubbles beyond the third nearest neighbor is small. In figure 6, we show the relative vertical velocity $R = V_y/V_1$ as a function of N, the number of bubbles, for several values of x_o. For a given separation distance, the rise velocity decreases with increasing N and levels off for $N > 3$. Thus, a three-bubble system describes well the basic morphology of an N-bubble system.

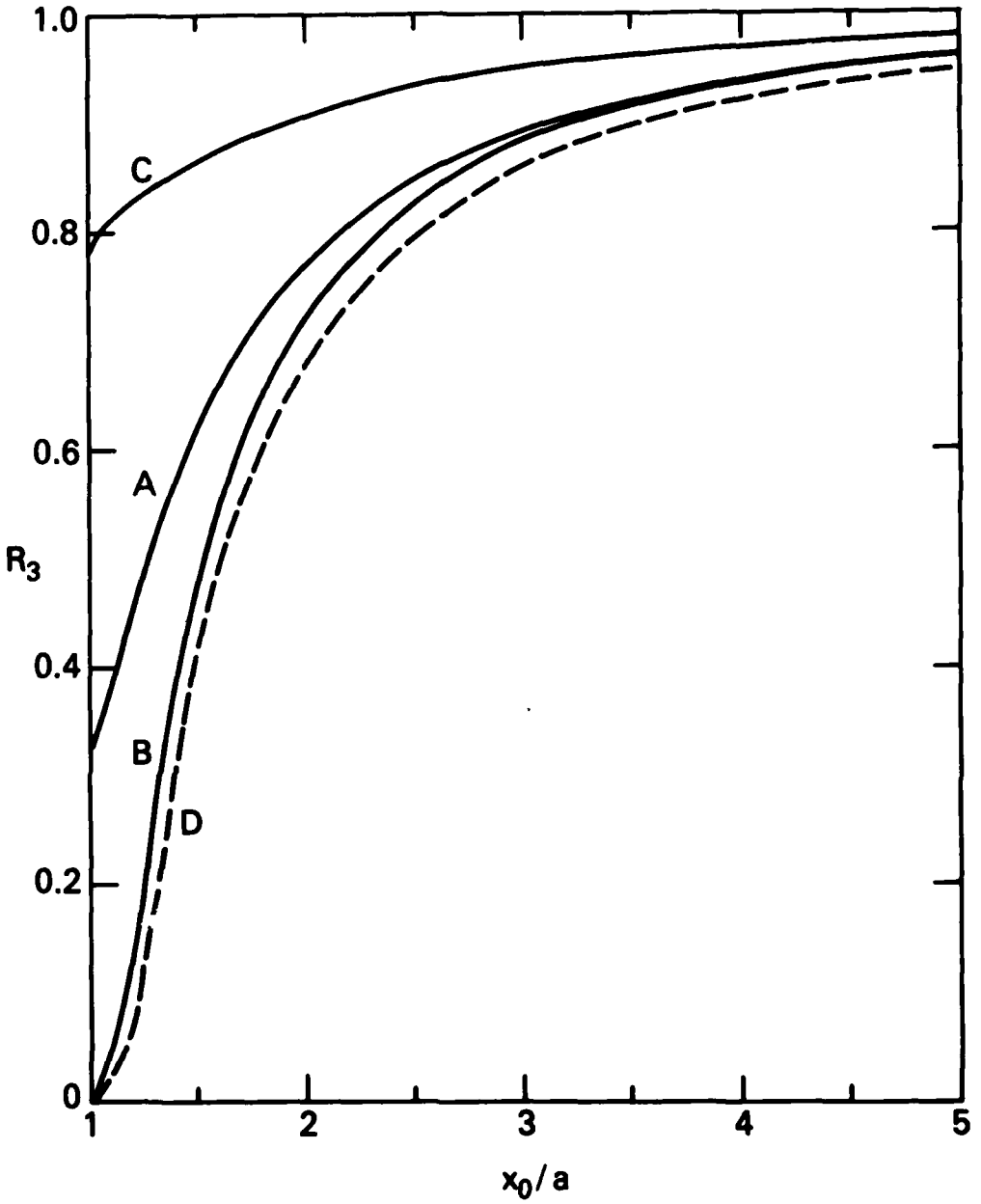

Fig. 5 The ratio R_3 of the vertical velocity V_y of a three-bubble system to the single-bubble rise velocity V_1, plotted versus x_o/a. The curves A, B, and C correspond to the points A, B, and C in figure 4. The curve D (dashed) corresponds to $R_5 = V_y/V_1$ at $x = a$ in a five-bubble system, to be compared with the curve B.

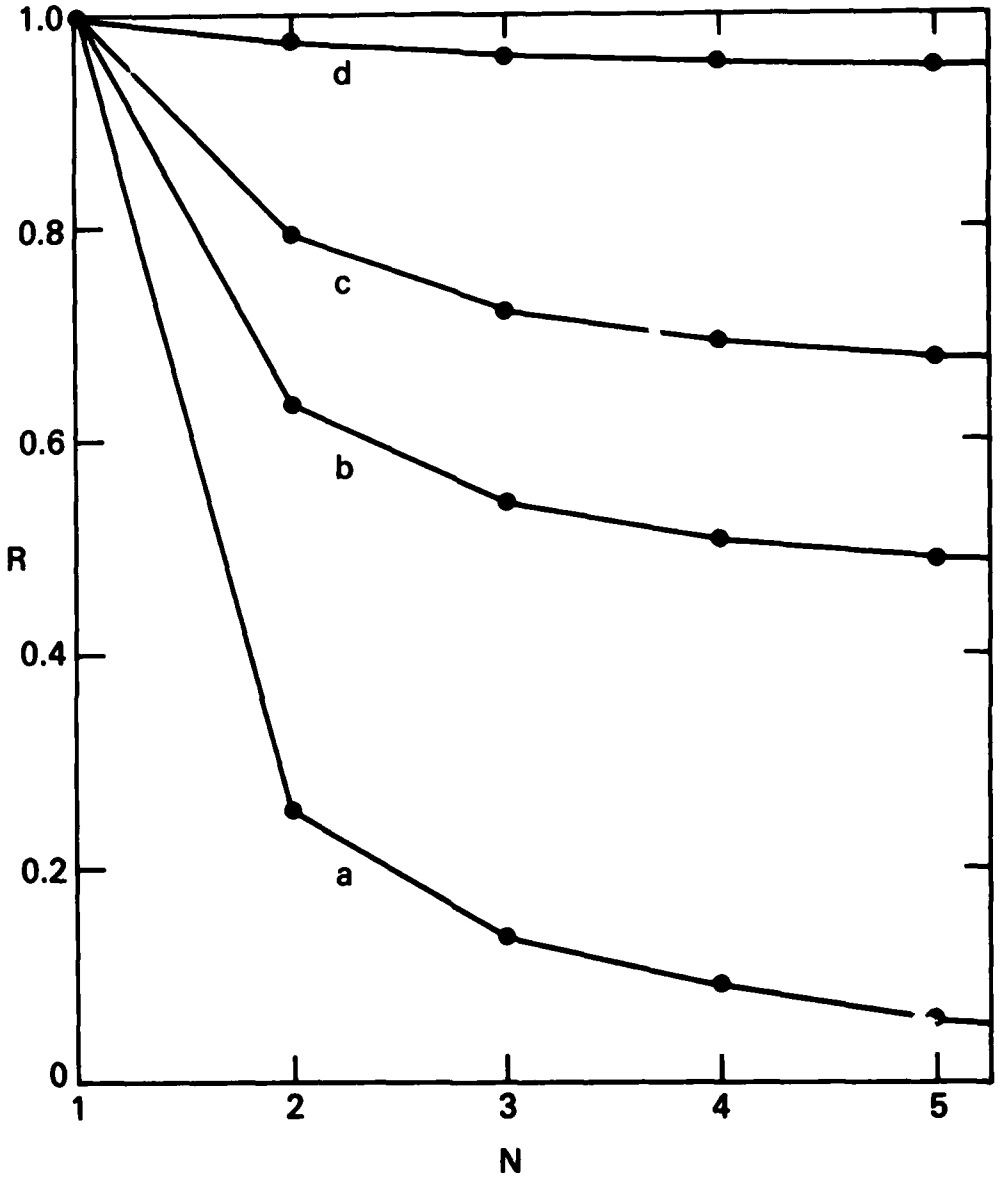

Fig. 6 $R = V_y/V_l$ versus N, the number of bubbles, evaluated inside at $x = x_o - a$ for the two-bubble case and at $x = a$ for all others. K = 0. The separation distances ($2x_o$) are (a) $2x_o = 2.5a$, (b) $2x_o = 3.2a$, (c) $2x_o = 4.0a$, and (d) $2x_o = 10a$.

Figures 3 and 5 show that the vertical drift velocity of a bubble is a sensitive function of the separation distance ($2x_o$) except for relativly large values ($2x_o/a \gtrsim 6$). In the context of the Rayleigh-Taylor instability, this implies that the electric field configuration and the drift velocities may depend sensitively on wavelengths ($2x_o$).

As a general remark, we point out that the preceding results derived for plasma density depletions for which $K < 1$ are also applicable to plasma density enhancements (clouds) for which $K > 1$. Calculations for the cloud case show that the electric field configurations are qualitatively similar to that of the bubble case (figures 2 and 4). In particular, the electric field inside the clouds experiences the greatest reduction in the regions facing the neighboring clouds. However, the boundary condition $K(E_{in})_\perp = (E_{out})_\perp$ implies that $(E_{in})_\perp$ is smaller than $(E_{out})_\perp$ by a factor of K^{-1} for clouds. Thus, for a given separation distance $2x_o$, the relative distortion in the electric field lines inside a cloud is less pronounced than in a bubble.

Finally, in figure 7, we have plotted the vertical drift velocity versus $K \equiv n_1/n_2$ for a two-bubble ($K < 1$) and two-cloud ($K > 1$) system. The velocity is calculated at $x = \pm (x_o - a)$ (point A in figure 2) and is upward for bubbles and downward for clouds. The velocity is normalized to V_1 (equation (27)) for each value of K. Note that the point with $K = 1$ does not exist for each line. For $K = 1$, the ionosphere is not disturbed and there is no bubble or cloud drifting vertically. This is born out by the fact that the drift velocity vanishes for a single-bubble (cloud) and any multi-bubble (cloud) system. Clearly, the velocities vanish differently for different separation distances. Mathematically, the ratio of the vertical drift velocity $V_y = c(E_x^* - E_o)/B_o$ to the single-bubble (cloud) drift velocity V_1 has the limit

$$\frac{V_y}{V_1} = -\left[1 - \frac{2}{1+K}\, a^2 f(x + x_o, y)\right]$$

as $K \to 1$. The circled points in figure 7 correspond to the absolute value of the quantity which has no physical meaning.

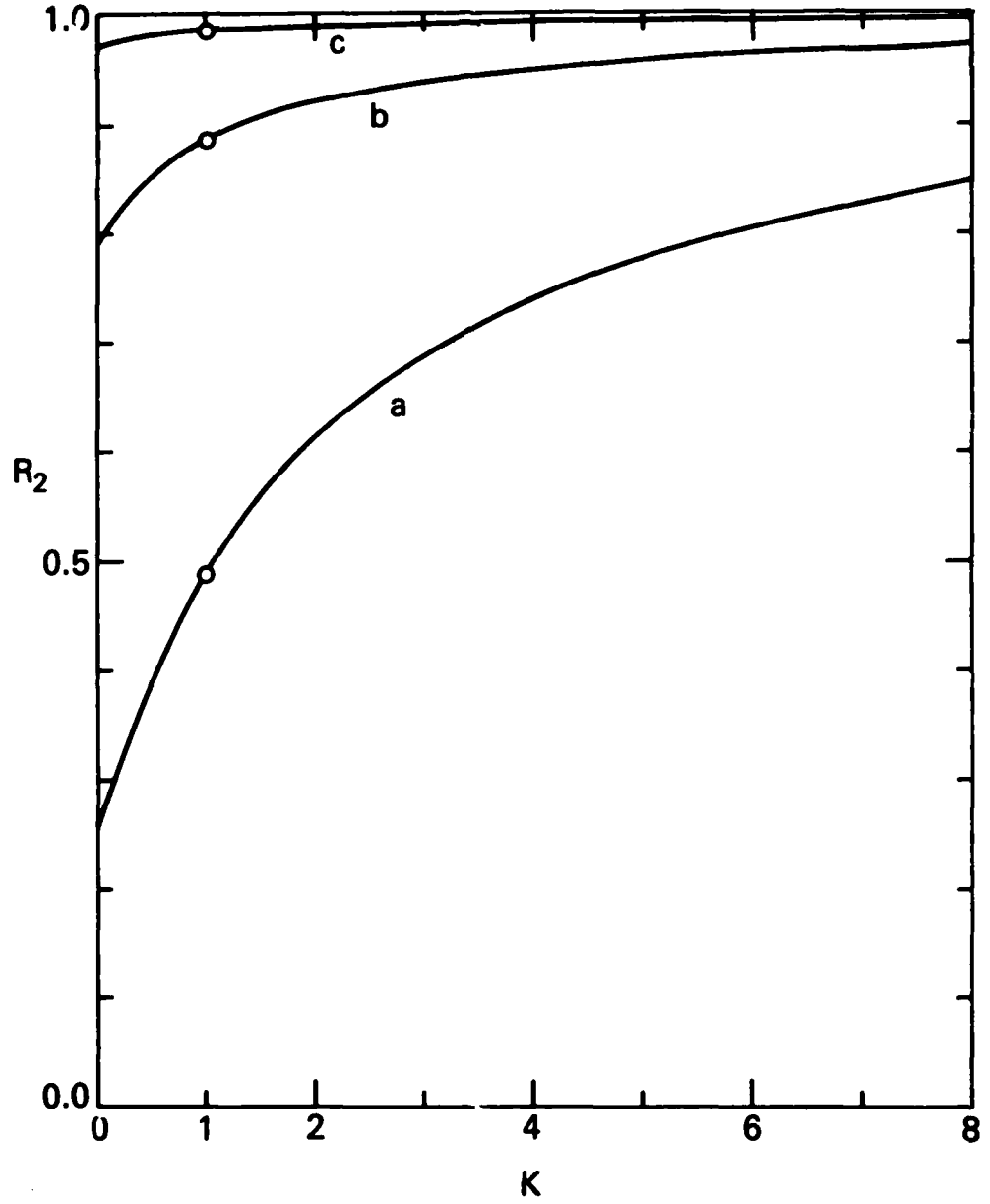

Fig. 7 $R_2 = V_y/V_1$ versus. K for two-bubble (K < 1) and two-cloud (K > 1) systems. The separation distances ($2x_o$) are (a) $2x_o = 2.5a$, (b) $2x_o = 4a$, and (c) $2x_o = 10a$.

IV. SUMMARY AND DISCUSSION

In the preceding sections, we have solved the current conservation equation (1) with quasi-neutrality for two-bubble and three-bubble systems using a dielectric analogy. These two configurations include the dominant near-neighbor interaction and can model the essential morphology of the multi-bubble systems described. This is demonstrated by actually calculating the field including up to five bubbles. The solutions are exact, satisfying the specified boundary conditions on all the multiple disconnected boundary surfaces and at infinity.

Equations (19), (20), (24) and (25) give the solution of the two-bubble system as a superposition of image line dipole moments. Similar expressions are obtained for three- and N-bubble (cloud) systems (N > 3). In all cases, the interaction is dominated by the nearest neighbors and is sensitive to the separation distance ($2x_o$) between bubbles. An important result is that the electric field inside the bubbles is generally highly non-uniform so that the multi-bubble and multi-cloud systems are not steady-state configurations even with piecewise constant density profiles (figures 2 and 4). Moreover, the electric field inside the bubbles is significantly weaker than that in a one-bubble system so that the vertical drift velocity relative to the undisturbed ionosphere is slower than the one-bubble case (equation (27) and figures 3 and 5). For moderately small center-to-center separation distances, $2x_o \lesssim 6a$, the reduction in the rise velocity is substantial. This implies that the electric field configuration and the $\underline{E} \times \underline{B}$ drift velocity may depend sensitively on the wavelengths of instabilities causing the initial density fluctuations (e.g., the Rayleigh-Taylor instability). In particular, the bubbles with smaller wavelength-to-radius ratio would rise more slowly and be distorted more strongly. This conclusion may be particularly applicable to the initial linear or early-time non-linear stages of the evolution. It has also been shown that in some regions inside bubbles, the horizontal drift velocity may be comparable to the vertical drift velocity with $|E_y^*/(E_x^*-E_o)|$ as large as 1/2 (Sections II and III).

A corollary that follows from the non-uniform electric field in the bubbles is that the polarization induced $\underline{E} \times \underline{B}$ drift velocity is sheared

and that a component of the electric field parallel to the local density gradient is developed in the leading edges of the bubbles. For the simple piecewise constant density profiles used for our analysis, the density gradient is not well defined. In a more realistic density profile, however, some previous model calculations indicate that the electric field component parallel to the density gradient has stabilizing influences on the Rayleigh-Taylor instability [Guzdar et al., 1982] and the $\underline{E} \times \underline{B}$ drift instability [Perkins and Doles, 1975; Huba et al., 1982). More specifically, these calculations show that velocity shear preferentially stabilizes the short wavelength modes. In light of these results, we suggest that the bifurcation behavior of bubbles and clouds may be inhibited by the presence of nearby bubbles (clouds).

The emphasis of our analysis has primarily been on plasma density depletions (bubbles). However, plasma density enhancements (clouds and striation fingers) can also be treated in a similar fashion [Scannapieco and Ossakow, 1976; Scannapieco et al., 1976; Ossakow and Chaturvedi, 1978]. If a cloud exists in the equatorial or low latitude region, the preceding results are all applicable with the replacement of $K > 1$ ($K < 1$ for bubbles) where $K = n_1/n_2$. In particular, as the backside of an initial cloud begins to bifurcate, the small x_o/a and small N results may be applicable. One point to note is that the electric field inside a two- and three-cloud system with a piecewise constant density profile is similar to that shown in figure 2 and 4 with weaker field strength in the regions facing the neighboring clouds. However, the boundary condition $K(E_{in})_\perp = (E_{out})_\perp$ implies that $(E_{in})_\perp$ is smaller than $(E_{out})_\perp$ by a factor of K^{-1} for clouds. As a result, the distortion in the electric field lines inside a cloud is less pronounced than in a bubble.

ACKNOWLEDGEMENTS

We would like to thank Drs. P. Chaturvedi, E. Overman, N. Zabusky, and S. Zalesak for useful discussions. This work has been supported by DNA and ONR.

REFERENCES

Anderson, D.N., and G. Haerendel, The motion of depleted plasma regions in the equatorial ionosphere, J. Geophys. Res., 84, 1251, 1979.

Balsley, B.B., G. Haerendel, and R.A. Greenwald, Equatorial spread F, recent observations and a new interpretation, J. Geophys. Res., 77, 5625, 1972.

Chaturvedi, P.K., and P. Kaw, Steady state finite amplitude Rayleigh-Taylor modes in Spread F, Geophys. Res. Lett., 2, 381, 1975a.

Chaturvedi, P.K., and P. Kaw, Correction, Geophys. Res. Lett., 2, 499, 1975b.

Dungey, J.W., Convective diffusion in the equatorial F region, J. Atmos. Terr. Phys., 9, 304, 1956.

Fejer, B.G. and M.C. Kelley, Ionospheric irregularities, Rev. Geophys. Space Phys., 18, 401, 1980.

Guzdar, P.N., P. Satyanarayana, J.D. Huba and S.L. Ossakow, Influence of velocity shear on Rayleigh-Taylor instability, Geophys. Res. Lett., 9, 547, 1982.

Haerendel, G., Theory of equatorial spread F, preprint, Max-Planck Inst. fur Astrophys., Munich, 1973.

Hanson, W.B., and J. Santani, Large N_i gradients below the equatorial F peak, J. Geophys. Res., 78, 1167, 1973.

Huba, J.D., S.L. Ossakow, P. Satyanarayana, and P.N. Guzdar, Linear theory of the $\underline{E} \times \underline{B}$ instability with an inhomogeneous electric field, J. Geophys. Res. (accepted for publication 1982).

Hudson, M.K., and C.F. Kennel, Linear theory of equatorial spread-F, J. Geophys. Res., 80, 4581, 1975.

Hudson, M.K., Spread F bubbles: Nonlinear Rayleigh-Taylor mode in two dimensions, J. Geophys. Res., 83, 3189, 1978.

Kelley, M.C., G. Haerendel, H. Kappler, A. Valenzuela, B.B. Balsley, D.A. Carter, W.L. Ecklund, C.W. Carlson, B. Hausler, and R. Torbert, Evidence for a Rayleigh-Taylor type instability and upwelling of depleted density regions during equatorial spread F, Geophys. Res. Lett., 3, 448, 1976.

Kelley, M.C., and J.P. McClure, Equatorial spread F: A review of recent experimental results, J. Atm. Terr. Phys., 43, 427, 1981.

Linson, L.M., and J.B. Workman, Formation of striations in ionospheric clouds, J. Geophys. Res., 75, 3211, 1970.

Longmire, C.L., On the motion of artificial ion clouds, Los Alamos Nuclear Corp. Report, LANC-N-11, 1970.

McClure, J.P., W.B. Hanson, and J.F. Hoffman, Plasma bubbles and irregularities in the equatorial ionosphere, J. Geophys. Res., 82, 2650, 1977.

Ossakow, S.L., and P.K. Chaturvedi, Morphological studies of rising equatorial spread F bubbles, J. Geophys. Res., 83, 2085, 1978.

Ossakow, S.L., Ionospheric irregularities, Rev. Geophys. Space Phys., 17, 521, 1979.

Ossakow, S.L., S.T. Zalesak, B.E. McDonald, and P.K. Chaturvedi, nonlinear equatorial spread F: Dependence on altitude of the F peak and bottomside background electron density gradient scale length, J. Geophys. Res., 84, 17, 1979.

Ossakow, S.L., Spread F theories - a review, J. Atmos. Terr. Phys., 43, 437, 1981.

Ossakow, S.L., M.J. Keskinen, and S.T. Zalesak, Ionospheric irregularity physics modelling, AIAA-82-0147, January 1982.

Ott, E., Theory of Rayleigh-Taylor bubbles in the equatorial ionosphere, J. Geophys. Res., 83, 2006, 1978.

Overman, E., N.J. Zabusky, and S.L. Ossakow, Ionospheric plasma cloud dynamics via regularized contour dynamics: I. Stability and nonlinear evolution of one contour models, Phys. Fluids (accepted for publication) 1982.

Perkins, F.W., N.J. Zabusky, and J.H. Doles III, Deformation and striation of plasma clouds in the ionosphere, 1., J. Geophys. Res., 78, 697, 1973.

Perkins, F.W., and J.H. Doles III, Velocity shear and the E x B instability, J. Geophys. Res., 80, 211, 1975.

Scannapieco, A.J., and S.L. Ossakow, Nonlinear equatorial spread F, Geophys. Res. Lett., 3, 451, 1976.

Scannapieco, A.J., S.L. Ossakow, S.R. Goldman, and J.M. Pierre, Plasma cloud late time striation spectra, J. Geophys. Res., 81, 6037, 1976.

Smythe, W.R., Static and Dynamic Electricity, Third edition, p. 95, McGraw-Hill Book Company, New York, 1968.

Szuszczewicz, E.P., R.T. Tsunoda, R. Narcisi, and J.C. Holmes, Coincident radar and rocket observations of equatorial spread F, Geophys. Res. Lett., 7, 537, 1980.

Szuszczewicz, E.P., R.T. Tsunoda, R. Narcisi, and J.C. Holmes, PLUMEX II: A second set of coincident radar and rocket observatios of equatorial spread F, Geophys. Res. Lett., 8, 803, 1981.

Volk, H.J., and G. Haerendel, Striation in ionospheric clouds, J. Geophys. Res., 76, 454, 1971.

Woodman, R.F. and C. LaHoz, Radar observations of equatorial irregularities, J. Geophys. Res., 81, 5447, 1976.

Zalesak, S.T., and S.L. Ossakow, Nonlinear equatorial spread F: Spatially large bubbles resulting from large horizontal scale initial perturbations, J. Geophys. Res., 85, 2131, 1980.

Zalesak, S.T., S.L. Ossakow, and P.K. Chaturvedi, Nonlinear equatorial spread F: The effect of neutral winds and background Pedersen conductivity, J. Geophys. Res., 87, 151, 1982.

DISTRIBUTION LIST

DEPARTMENT OF DEFENSE

ASSISTANT SECRETARY OF DEFENSE
COMM, CMD, CONT 7 INTELL
WASHINGTON, D.C. 20301
01CY ATTN J. BABCOCK
01CY ATN M. EPSTEIN

DIRECTOR
COMMAND CONTROL TECHNICAL CENTER
PENTAGON RM BE 685
WASHINGTON, D.C. 20301
01CY ATTN C-650
01CY ATTN C-312 R. MASON

DIRECTOR
DEFENSE ADVANCED RSCH PROJ AGENCY
ARCHITECT BUILDING
1400 WILSON BLVD.
ARLINGTON, VA. 22209
01CY ATTN NUCLEAR MONITORING RESEARCH
01CY ATTN STRATEGIC TECH OFFICE

DEFENSE COMMUNICATION ENGINEER CENTER
1860 WIEHLE AVENUE
RESTON, VA. 22090
01CY ATTN CODE R410
01CY ATTN CODE R812

DIRECTOR
DEFENSE COMMUNICATIONS AGENCY
WASHINGTON, D.C. 20305
(ADR CNWDI: ATTN CODE 240 FOR)
01CY ATTN CODE 101B

DEFENSE TECHNICAL INFORMATION CENTER
CAMERON STATION
ALEXANDRIA, VA 22314
02CY

DIRECTOR
DEFENSE NUCLEAR AGENCY
WASHINGTON, D.C. 20305
01CY ATTN STVL
04CY ATTN TITL
01CY ATTN DDST
03CY ATTN RAAE

COMMANDER
FIELD COMMAND
DEFENSE NUCLEAR AGENCY
KIRTLAND, AFB, NM 87115
01CY ATTN FCPR

DIRECTOR
INTERSERVICE NUCLEAR WEAPONS SCHOOL
KIRTLAND AFB, NM 87115
01CY ATTN DOCUMENT CONTROL

JOINT CHIEFS OF STAFF
WASHINGTON, D.C. 20301
01CY ATTN J-3 WWMCCS EVALUATION OFFICE

DIRECTOR
JOINT STRAT TGT PLANNING STAFF
OFFUTT AFB
OMAHA, NB 68113
01CY ATTN JLTW-2
01CY ATTN JPST G. GOETZ

CHIEF
LIVERMORE DIVISION FLD COMMAND DNA
DEPARTMENT OF DEFENSE
LAWRENCE LIVERMORE LABORATORY
P.O. BOX 808
LIVERMORE, CA 94550
01CY ATTN FCPRL

COMMANDANT
NATO SCHOOL (SHAPE)
APO NEW YORK 09172
01CY ATTN U.S. DOCUMENTS OFFICER

UNDER SECY OF DEF FOR RSCH & ENGRG
DEPARTMENT OF DEFENSE
WASHINGTON, D.C. 20301
01CY ATTN STRATEGIC & SPACE SYSTEMS (OS)

WWMCCS SYSTEM ENGINEERING ORG
WASHINGTON, D.C. 20305
01CY ATTN R. CRAWFORD

COMMANDER/DIRECTOR
ATMOSPHERIC SCIENCES LABORATORY
U.S. ARMY ELECTRONICS COMMAND
WHITE SANDS MISSILE RANGE, NM 88002
01CY ATTN DELAS-EO F. NILES

DIRECTOR
BMD ADVANCED TECH CTR
HUNTSVILLE OFFICE
P.O. BOX 1500
HUNTSVILLE, AL 35807
01CY ATTN ATC-T MELVIN T. CAPPS
01CY ATTN ATC-O W. DAVIES
01CY ATTN ATC-R DON RUSS

PROGRAM MANAGER
BMD PROGRAM OFFICE
5001 EISENHOWER AVENUE
ALEXANDRIA, VA 22333
01CY ATTN DACS-BMT J. SHEA

CHIEF C-E- SERVICES DIVISION
U.S. ARMY COMMUNICATIONS CMD
PENTAGON RM 1B269
WASHINGTON, D.C. 20310
01CY ATTN C- E-SERVICES DIVISION

COMMANDER
FRADCOM TECHNICAL SUPPORT ACTIVITY
DEPARTMENT OF THE ARMY
FORT MONMOUTH, N.J. 07703
01CY ATTN DRSEL-NL-RD H. BENNET
01CY ATTN DRSEL-PL-ENV H. BOMKE
01CY ATTN J.E. QUIGLEY

COMMANDER
HARRY DIAMOND LABORATORIES
DEPARTMENT OF THE ARMY
2800 POWDER MILL ROAD
ADELPHI, MD 20783
(CNWDI-INNER ENVELOPE: ATTN: DELHD-RBH)
01CY ATTN DELHD-TI M. WEINER
01CY ATTN DELHD-RB R. WILLIAMS
01CY ATTN DELHD-NP F. WIMENITZ
01CY ATTN DELHD-NP C. MOAZED

COMMANDER
U.S. ARMY COMM-ELEC ENGRG INSTAL AGY
FT. HUACHUCA, AZ 85613
01CY ATTN CCC-EMEO GEORGE LANE

COMMANDER
U.S. ARMY FOREIGN SCIENCE & TECH CTR
220 7TH STREET, NE
CHARLOTTESVILLE, VA 22901
01CY ATTN DRXST-SD
01CY ATTN R. JONES

COMMANDER
U.S. ARMY MATERIAL DEV & READINESS CMD
5001 EISENHOWER AVENUE
ALEXANDRIA, VA 22333
01CY ATTN DRCLDC J.A. BENDER

COMMANDER
U.S. ARMY NUCLEAR AND CHEMICAL AGENCY
7500 BACKLICK ROAD
BLDG 2073
SPRINGFIELD, VA 22150
01CY ATTN LIBRARY

DIRECTOR
U.S. ARMY BALLISTIC RESEARCH LABORATORY
ABERDEEN PROVING GROUND, MD 21005
01CY ATTN TECH LIBRARY EDWARD BAICY

COMMANDER
U.S. ARMY SATCOM AGENCY
FT. MONMOUTH, NJ 07703
01CY ATTN DOCUMENT CONTROL

COMMANDER
U.S. ARMY MISSILE INTELLIGENCE AGENCY
REDSTONE ARSENAL, AL 35809
01CY ATTN JIM GAMBLE

DIRECTOR
U.S. ARMY TRADOC SYSTEMS ANALYSIS ACTIVIT
WHITE SANDS MISSILE RANGE, NM 88002
01CY ATTN ATAA-SA
01CY ATTN TCC/F. PAYAN JR.
01CY ATTN ATTA-TAC LTC J. HESSE

COMMANDER
NAVAL ELECTRONIC SYSTEMS COMMAND
WASHINGTON, D.C. 20360
01CY ATTN NAVALEX 034 T. HUGHES
01CY ATTN PME 117
01CY ATTN PME 117-T
01CY ATTN CODE 5011

COMMANDING OFFICER
NAVAL INTELLIGENCE SUPPORT CTR
4301 SUITLAND ROAD, BLDG. 5
WASHINGTON, D.C. 20390
01CY ATTN MR. DUBBIN STIC 12
01CY ATTN NISC-50
01CY ATTN CODE 5404 J. GALET

COMMANDER
NAVAL OCCEAN SYSTEMS CENTER
SAN DIEGO, CA 92152
03CY ATTN CODE 532 W. MOLER
01CY ATTN CODE 0230 C. BAGGETT
01CY ATTN CODE 81 R. EASTMAN

DIRECTOR
NAVAL RESEARCH LABORATORY
WASHINGTON, D.C. 20375
01CY ATTN CODE 4700 S. L. Ossakow
26 CYS IF UNCLASS. 1 CY IF CLASS)
01CY ATTN CODE 4701 JACK D. BROWN
01CY ATTN CODE 4780 BRANCH HEAD (100
CYS IF UNCLASS, 1 CY IF CLASS)
01CY ATTN CODE 7500
01CY ATTN CODE 7550
01CY ATTN CODE 7580
01CY ATTN CODE 7551
01CY ATTN CODE 7555
01CY ATTN CODE 4730 E. MCLEAN
01CY ATTN CODE 4187
20CY ATTN CODE 2628

COMMANDER
NAVAL SEA SYSTEMS COMMAND
WASHINGTON, D.C. 20362
01CY ATTN CAPT R. PITKIN

COMMANDER
NAVAL SPACE SURVEILLANCE SYSTEM
DAHLGREN, VA 22448
01CY ATTN CAPT J.H. BURTON

OFFICER-IN-CHARGE
NAVAL SURFACE WEAPONS CENTER
WHITE OAK, SILVER SPRING, MD 20910
01CY ATTN CODE F31

DIRECTOR
STRATEGIC SYSTEMS PROJECT OFFICE
DEPARTMENT OF THE NAVY
WASHINGTON, D.C. 20376
01CY ATTN NSP-2141
01CY ATTN NSSP-2722 FRED WIMBERLY

COMMANDER
NAVAL SURFACE WEAPONS CENTER
DAHLGREN LABORATORY
DAHLGREN, VA 22448
01CY ATTN CODE DF-14 R. BUTLER

OFFICER OF NAVAL RESEARCH
ARLINGTON, VA 22217
01CY ATTN CODE 465
01CY ATTN CODE 461
01CY ATTN CODE 402
01CY ATTN CODE 420
01CY ATTN CODE 421

COMMANDER
AEROSPACE DEFENSE COMMAND/DC
DEPARTMENT OF THE AIR FORCE
ENT AFB, CO 80912
01CY ATTN DC MR. LONG

COMMANDER
AEROSPACE DEFENSE COMMAND/XPD
DEPARTMENT OF THE AIR FORCE
ENT AFB, CO 80912
01CY ATTN XPDQQ
01CY ATTN XP

AIR FORCE GEOPHYSICS LABORATORY
HANSCOM AFB, MA 01731
01CY ATTN OPR HAROLD GARDNER
01CY ATTN LKB KENNETH S.W. CHAMPION
01CY ATTN OPR ALVA T. STAIR
01CY ATTN PHP JULES AARONS
01CY ATTN PHD JURGEN BUCHAU
01CY ATTN PHD JOHN P. MULLEN

AF WEAPONS LABORATORY
KIRTLAND AFT, NM 87117
01CY ATTN SUL
01CY ATTN CA ARTHUR H. GUENTHER
01CY ATTN NTYCE 1LT. G. KRAJEI

AFTAC
PATRICK AFB, FL 32925
01CY ATTN TF/MAJ WILEY
01CY ATTN TN

AIR FORCE AVIONICS LABORATORY
WRIGHT-PATTERSON AFB, OH 45433
01CY ATTN AAD WADE HUNT
01CY ATTN AAD ALLEN JOHNSON

DEPUTY CHIEF OF STAFF
RESEARCH, DEVELOPMENT, & ACQ
DEPARTMENT OF THE AIR FORCE
WASHINGTON, D.C. 20330
01CY ATTN AFRDQ

HEADQUATERS
ELECTRONIC SYSTEMS DIVISION/XR
DEPARTMENT OF THE AIR FORCE
HANSCOM AFB, MA 01731
01CY ATTN XR J. DEAS

HEADQUATERS
ELECTRONIC SYSTEMS DIVISION/YSEA
DEPARTMENT OF THE AIR FORCE
HANSCOM AFB, MA 01732
01CY ATTN YSEA

HEADQUATERS
ELECTRONIC SYSTEMS DIVISION/DC
DEPARTMENT OF THE AIR FORCE
HANSCOM AFB, MA 01731
01CY ATTN DCKC MAJ J.C. CLARK

COMMANDER
FOREIGN TECHNOLOGY DIVISION, AFSC
WRIGHT-PATTERSON AFB, OH 45433
01CY ATTN NICD LIBRARY
01CY ATTN ETDP B. BALLARD

COMMANDER
ROME AIR DEVELOPMENT CENTER, AFSC
GRIFFISS AFB, NY 13441
01CY ATTN DOC LIBRARY/TSLD
01CY ATTN OCSE V. COYNE

SAMSO/SZ
POST OFFICE BOX 92960
WORLDWAY POSTAL CENTER
LOS ANGELES, CA 90009
(SPACE DEFENSE SYSTEMS)
01CY ATTN SZJ

STRATEGIC AIR COMMAND/XPFS
OFFUTT AFB, NB 68113
01CY ATTN XPFS MAJ B. STEPHAN
01CY ATTN ADWATE MAJ BRUCE BAUER
01CY ATTN NRT
01CY ATTN DOK CHIEF SCIENTIST

SAMSO/SK
P.O. BOX 92960
WORLDWAY POSTAL CENTER
LOS ANGELES, CA 90009
01CY ATTN SKA (SPACE COMM SYSTEMS)
M. CLAVIN

SAMSO/MN
NORTON AFB, CA 92409
(MINUTEMAN)
01CY ATTN MNNL LTC KENNEDY

COMMANDER
ROME AIR DEVELOPMENT CENTER, AFSC
HANSCOM AFB, MA 01731
01CY ATTN EEP A. LORENTZEN

DEPARTMENT OF ENERGY
LIBRARY ROOM G-042
WASHINGTON, D.C. 20545
01CY ATTN DOC CON FOR A. LABOWITZ

DEPARTMENT OF ENERGY
ALBUQUERQUE OPERATIONS OFFICE
P.O. BOX 5400
ALBUQUERQUE, NM 87115
01CY ATTN DOC CON FOR D. SHERWOOD

EG&G, INC.
LOS ALAMOS DIVISION
P.O. BOX 809
LOS ALAMOS, NM 85544
01CY ATTN DOC CON FOR J. BREEDLOVE

UNIVERSITY OF CALIFORNIA
LAWRENCE LIVERMORE LABORATORY
P.O. BOX 808
LIVERMORE, CA 94550
01CY ATTN DOC CON FOR TECH INFO DEP
01CY ATTN DOC CON FOR L-389 R. OTT
01CY ATTN DOC CON FOR L-31 R. HAGER
01CY ATTN DOC CON FOR L-46 F. SEWAR

LOS ALAMOS NATIONAL LABORATORY
P.O. BOX 1663
LOS ALAMOS, NM 87545
01CY ATTN DOC CON FOR J. WOLCOTT
01CY ATTN DOC CON FOR R.F. TASCHEK
01CY ATTN DOC CON FOR E. JONES
01CY ATTN DOC CON FOR J. MALIK
01CY ATTN DOC CON FOR R. JEFFRIES
01CY ATTN DOC CON FOR J. ZINN
01CY ATTN DOC CON FOR P. KEATON
01CY ATTN DOC CON FOR D. WESTERVELT

SANDIA LABORATORIES
P.O. BOX 5800
ALBUQUERQUE, NM 87115
01CY ATTN DOC CON FOR W. BROWN
01CY ATTN DOC CON FOR A. THORNBROUG
01CY ATTN DOC CON FOR T. WRIGHT
01CY ATTN DOC CON FOR D. DAHLGREN
01CY ATTN DOC CON FOR 3141
01CY ATTN DOC CON FOR SPACE PROJECT

SANDIA LABORATORIES
LIVERMORE LABORATORY
P.O. BOX 969
LIVERMORE, CA 94550
01CY ATTN DOC CON FOR B. MURPHEY
01CY ATTN DOC CON FOR T. COOK

OFFICE OF MILITARY APPLICATION
DEPARTMENT OF ENERGY
WASHINGTON, D.C. 20545
01CY ATTN DOC CON DR. YO SONG

OTHER GOVERNMENT

DEPARTMENT OF COMMERCE
NATIONAL BUREAU OF STANDARDS
WASHINGTON, D.C. 20234
(ALL CORRES: ATTN SEC OFFICER FOR)
01CY ATTN R. MOORE

INSTITUTE FOR TELECOM SCIENCES
NATIONAL TELECOMMUNICATIONS & INFO ADMIN
BOULDER, CO 80303
01CY ATTN A. JEAN (UNCLASS ONLY)
01CY ATTN W. UTLAUT
01CY ATTN D. CROMBIE
01CY ATTN L. BERRY

NATIONAL OCEANIC & ATMOSPHERIC ADMIN
ENVIRONMENTAL RESEARCH LABORATORIES
DEPARTMENT OF COMMERCE
BOULDER, CO 80302
01CY ATTN R. GRUBB
01CY ATTN AERONOMY LAB G. REID

DEPARTMENT OF DEFENSE CONTRACTORS

AEROSPACE CORPORATION
P.O. BOX 92957
LOS ANGELES, CA 90009
01CY ATTN I. GARFUNKEL
01CY ATTN T. SALMI
01CY ATTN V. JOSEPHSON
01CY ATTN S. BOWER
01CY ATTN N. STOCKWELL
01CY ATTN D. OLSEN

ANALYTICAL SYSTEMS ENGINEERING CORP
5 OLD CONCORD ROAD
BURLINGTON, MA 01803
01CY ATTN RADIO SCIENCES

BERKELEY RESEARCH ASSOCIATES, INC.
P.O. BOX 983
BERKELEY, CA 94701
01CY ATTN J. WORKMAN
01CY ATTN C. PRETTIE

BOEING COMPANY, THE
P.O. BOX 3707
SEATTLE, WA 98124
01CY ATTN G. KEISTER
01CY ATTN D. MURRAY
01CY ATTN G. HALL
01CY ATTN J. KENNEY

BROWN ENGINEERING COMPANY, INC.
CUMMINGS RESEARCH PARK
HUNTSVILLE, AL 35807
01CY ATTN ROMEO A. DELIBERIS

CALIFORNIA AT SAN DIEGO, UNIV OF
P.O. BOX 6049
SAN DIEGO, CA 92106

CHARLES STARK DRAPER LABORATORY, INC.
555 TECHNOLOGY SQUARE
CAMBRIDGE, MA 02139
01CY ATTN D.B. COX
01CY ATTN J.P. GILMORE

COMSAT LABORATORIES
LINTHICUM ROAD
CLARKSBURG, MD 20734
01CY ATTN G. HYDE

CORNELL UNIVERSITY
DEPARTMENT OF ELECTRICAL ENGINEERING
ITHACA, NY 14850
01CY ATTN D.T. FARLEY, JR.

ELECTROSPACE SYSTEMS, INC.
BOX 1359
RICHARDSON, TX 75080
01CY ATTN H. LOGSTON
01CY ATTN SECURITY (PAUL PHILLIPS)

ESL, INC.
495 JAVA DRIVE
SUNNYVALE, CA 94086
01CY ATTN J. ROBERTS
01CY ATTN JAMES MARSHALL

GENERAL ELECTRIC COMPANY
SPACE DIVISION
VALLEY FORGE SPACE CENTER
GODDARD BLVD KING OF PRUSSIA
P.O. BOX 8555
PHILADELPHIA, PA 19101
01CY ATTN M.H. BORTNER SPACE SCI LAB

GENERAL ELECTRIC COMPANY
P.O. BOX 1122
SYRACUSE, NY 13201
01CY ATTN F. REIBERT

GENERAL ELECTRIC TECH SERVICES CO., INC
HMES
COURT STREET
SYRACUSE, NY 13201
01CY ATTN G. MILLMAN

GENERAL RESEARCH CORPORATION
SANTA BARBARA DIVISION
P.O. BOX 6770
SANTA BARBARA, CA 93111
01CY ATTN JOHN ISE, JR.
01CY ATTN JOEL GARBARINO

GEOPHYSICAL INSTITUTE
UNIVERSITY OF ALASKA
FAIRBANKS, AK 99701
(ALL CLASS ATTN: SECURITY OFFICER)
01CY ATTN T.N. DAVIS (UNCLASS ONLY)
01CY ATTN TECHNICAL LIBRARY
01CY ATTN NEAL BROWN (UNCLASS ONLY)

GTE SYLVANIA, INC.
ELECTRONICS SYSTEMS GRP-EASTERN DIV
77 A STREET
NEEDHAM, MA 02194
01CY ATTN MARSHALL CROSS

HSS, INC.
2 ALFRED CIRCLE
BEDFORD, MA 01730
01CY ATTN DONALD HANSEN

ILLINOIS, UNIVERSITY OF
107 COBLE HALL
150 DAVENPORT HOUSE
CHAMPAIGN, IL 61820
(ALL CORRES ATTN DAN MCCLELLAND)
01CY ATTN K. YEH

INSTITUTE FOR DEFENSE ANALYSES
400 ARMY-NAVY DRIVE
ARLINGTON, VA 22202
01CY ATTN J.M. AEIN
01CY ATTN ERNEST BAUER
01CY ATTN HANS WOLFARD
01CY ATTN JOEL BENGSTON

INTL TEL & TELEGRAPH CORPORATION
500 WASHINGTON AVENUE
NUTLEY, NJ 07110
01CY ATTN TECHNICAL LIBRARY

JAYCOR
11011 TORREYANA ROAD
P.O. BOX 85154
SAN DIEGO, CA 92138
01CY ATTN J.L. SPERLING

JOHNS HOPKINS UNIVERSITY
APPLIED PHYSICS LABORATORY
JOHNS HOPKINS ROAD
LAURAL, MD 20810
01CY ATTN DOCUMENT LIBRARIAN
01CY ATTN THOMAS POTEMRA
01CY ATTN JOHN DASSOULAS

KAMAN SCIENCES CORP
P.O. BOX 7463
COLORADO SPRINGS, CO 80933
01CY ATTN T. MEAGHER

KAMAN TEMPO-CENTER FOR ADVANCED STUD:
816 STATE STREET (P.O DRAWER QQ)
SANTA BARBARA, CA 93102
01CY ATTN DASIAC
01CY ATTN TIM STEPHANS
01CY ATTN WARREN S. KNAPP
01CY ATTN WILLIAM MCNAMARA
01CY ATTN B. GAMBILL

LINKABIT CORP
10453 ROSELLE
SAN DIEGO, CA 92121
01CY ATTN IRWIN JACOBS

LOCKHEED MISSILES & SPACE CO., INC
P.O. BOX 504
SUNNYVALE, CA 94088
01CY ATTN DEPT 60-12
01CY ATTN D.R. CHURCHILL

LOCKHEED MISSILES & SPACE CO., INC.
3251 HANOVER STREET
PALO ALTO, CA 94304
01CY ATTN MARTIN WALT DEPT 52-12
01CY ATTN W.L. IMHOF DEPT 52-12
01CY ATTN RICHARD G. JOHNSON DEPT
01CY ATTN J.B. CLADIS DEPT 52-12

LOCKHEED MISSILE & SPACE CO., INC.
HUNTSVILLE RESEARCH & ENGR. CTR.
4800 BRADFORD DRIVE
HUNTSVILLE, AL 35807
ATTN DALE H. DIVIS

MARTIN MARIETTA CORP
ORLANDO DIVISION
P.O. BOX 5837
ORLANDO, FL 32805
01CY ATTN R. HEFFNER

M.I.T. LINCOLN LABORATORY
P.O. BOX 73
LEXINGTON, MA 02173
01CY ATTN DAVID M. TOWLE
01CY ATTN P. WALDRON
01CY ATTN L. LOUGHLIN
01CY ATTN D. CLARK

MCDONNEL DOUGLAS CORPORATION
5301 BOLSA AVENUE
HUNTINGTON BEACH, CA 92647
01CY ATTN N. HARRIS
01CY ATTN J. MOULE
01CY ATTN GEORGE MROZ
01CY ATTN W. OLSON
01CY ATTN R.W. HALPRIN
01CY ATTN TECHNICAL LIBRARY SERVICE

MISSION RESEARCH CORPORATION
735 STATE STREET
SANTA BARBARA, CA 93101
01CY ATTN P. FISCHER
01CY ATTN W.F. CREVIER
01CY ATTN STEVEN L. GUTSCHE
01CY ATTN D. SAPPENFIELD
01CY ATTN R. BOGUSCH
01CY ATTN R. HENDRICK
01CY ATTN RALPH KILB
01CY ATTN DAVE SOWLE
01CY ATTN F. FAJEN
01CY ATTN M. SCHEIBE
01CY ATTN CONRAD L. LONGMIRE
01CY ATTN WARREN A. SCHLUETER

MITRE CORPORATION, THE
P.O. BOX 208
BEDFORD, MA 01730
01CY ATTN JOHN MORGANSTERN
01CY ATTN G. HARDING
01CY ATTN C.E. CALLAHAN

MITRE CORP
WESTGATE RESEARCH PARK
1820 DOLLY MADISON BLVD
MCLEAN, VA 22101
01CY ATTN W. HALL
01CY ATTN W. FOSTER

PACIFIC-SIERRA RESEARCH CORP.
1456 CLOVERFIELD BLVD.
SANTA MONICA, CA 90404
01CY ATTN E.C. FIELD, JR.

PENNSYLVANIA STATE UNIVERSITY
IONOSPHERE RESEARCH LAB
318 ELECTRICAL ENGINEERING EAST
UNIVERSITY PARK, PA 16802
(NO CLASS TO THIS ADDRESS)
01CY ATTN IONOSPHERIC RESEARCH LAB

PHOTOMETRICS, INC.
442 MARRETT ROAD
LEXINGTON, MA 02173
01CY ATTN IRVING L. KOFSKY

PHYSICAL DYNAMICS, INC.
P.O. BOX 3027
BELLEVUE, WA 98009
01CY ATTN E.J. FREMOUW

PHYSICAL DYNAMICS, INC.
P.O. BOX 10367
OAKLAND, CA 94610
ATTN A. THOMSON

R & D ASSOCIATES
P.O. BOX 9695
MARINA DEL REY, CA 90291
01CY ATTN FORREST GILMORE
01CY ATTN BRYAN GABBARD
01CY ATTN WILLIAM B. WRIGHT, JR.
01CY ATTN ROBERT F. LELEVIER
01CY ATTN WILLIAM J. KARZAS
01CY ATTN H. ORY
01CY ATTN C. MACDONALD
01CY ATTN R. TURCO

RAND CORPORATION, THE
1700 MAIN STREET
SANTA MONICA, CA 90406
01CY ATTN CULLEN CRAIN
01CY ATTN ED BEDROZIAN

RAYTHEON CO.
528 BOSTON POST ROAD
SUDBURY, MA 01776
01CY ATTN BARBARA ADAMS

RIVERSIDE RESEARCH INSTITUTE
80 WEST END AVENUE
NEW YORK, NY 10023
01CY ATTN VINCE TRAPANI

SCIENCE APPLICATIONS, INC.
P.O. BOX 2351
LA JOLLA, CA 92038
01CY ATTN LEWIS M. LINSON
01CY ATTN DANIEL A. HAMLIN
01CY ATTN E. FRIEMAN
01CY ATTN E.A. STRAKER
01CY ATTN CURTIS A. SMITH
01CY ATTN JACK MCDOUGALL

SCIENCE APPLICATIONS, INC
1710 GOODRIDGE DR.
MCLEAN, VA 22102
ATTN: J. COCKAYNE

SRI INTERNATIONAL
333 RAVENSWOOD AVENUE
MENLO PARK, CA 94025
01CY ATTN DONALD NEILSON
01CY ATTN ALAN BURNS
01CY ATTN G. SMITH
01CY ATTN L.L. COBB
01CY ATTN DAVID A. JOHNSON
01CY ATTN WALTER G. CHESNUT
01CY ATTN CHARLES L. RINO
01CY ATTN WALTER JAYE
01CY ATTN M. BARON
01CY ATTN RAY L. LEADABRAND
01CY ATTN G. CARPENTER
01CY ATTN G. PRICE
01CY ATTN J. PETERSON
01CY ATTN R. HAKE, JR.
01CY ATTN V. GONZALES
01CY ATTN D. MCDANIEL

STEWART RADIANCE LABORATORY
UTAH STATE UNIVERSITY
1 DE ANGELO DRIVE
BEDFORD, MA 01730
01CY ATTN J. ULWICK

TECHNOLOGY INTERNATIONAL CORP
75 WIGGINS AVENUE
BEDFORD, MA 01730
01CY ATTN W.P. BOQUIST

TRW DEFENSE & SPACE SYS GROUP
ONE SPACE PARK
REDONDO BEACH, CA 90278
01CY ATTN R. K. PLEBUCH
01CY ATTN S. ALTSCHULER
01CY ATTN D. DEE

VISIDYNE
SOUTH BEDFORD STREET
BURLINGTON, MASS 01803
01CY ATTN W. REIDY
01CY ATTN J. CARPENTER
01CY ATTN C. HUMPHREY

IONOSPHERIC MODELING DISTRIBUTION LIST
(UNCLASSIFIED ONLY)

PLEASE DISTRIBUTE ONE COPY TO EACH OF THE FOLLOWING PEOPLE (UNLESS OTHERWISE NOTED)

NAVAL RESEARCH LABORATORY
WASHINGTON, D.C. 20375
DR. P. MANGE - CODE 4101
DR. E. SZUSZCZEWICZ - CODE 4187
DR. J. GOODMAN - CODE 4180
DR. P. RODRIGUEZ - CODE 4187

A.F. GEOPHYSICS LABORATORY
L.G. HANSCOM FIELD
BEDFORD, MA 01730
DR. T. ELKINS
DR. W. SWIDER
MRS. R. SAGALYN
DR. J.M. FORBES
DR. T.J. KENESHEA
DR. J. AARONS
DR. H. CARLSON
DR. J. JASPERSE

CORNELL UNIVERSITY
ITHACA, NY 14850
DR. W.E. SWARTZ
DR. R. SUDAN
DR. D. FARLEY
DR. M. KELLEY

HARVARD UNIVERSITY
HARVARD SQUARE
CAMBRIDGE, MA 02138
DR. M.B. McELROY
DR. R. LINDZEN

INSTITUTE FOR DEFENSE ANALYSIS
400 ARMY/NAVY DRIVE
ARLINGTON, VA 22202
DR. E. BAUER

MASSACHUSETTS INSTITUTE OF TECHNOLOGY
PLASMA FUSION CENTER
LIBRARY, NW16-262
CAMBRIDGE, MA 02139

NASA
Code 961
GODDARD SPACE FLIGHT CENTER
GREENBELT, MD 20771
DR. R.F. BENSON
DR. K. MAEDA
Dr. S. Curtis
Dr. M. Dubin

NATIONAL TECHNICAL INFORMATION CENTER
CAMERON STATION
ALEXANDRIA, VA 22314
12CY ATTN TC

COMMANDER
NAVAL AIR SYSTEMS COMMAND
DEPARTMENT OF THE NAVY
WASHINGTON, D.C. 20360
DR. T. CZUBA

COMMANDER
NAVAL OCEAN SYSTEMS CENTER
SAN DIEGO, CA 92152
MR. R. ROSE - CODE 5321

NOAA
DIRECTOR OF SPACE AND ENVIRONMENTAL LABORATORY
BOULDER, CO 80302
DR. A. GLENN JEAN
DR. G.W. ADAMS
DR. D.N. ANDERSON
DR. K. DAVIES
DR. R. F. DONNELLY

OFFICE OF NAVAL RESEARCH
800 NORTH QUINCY STREET
ARLINGTON, VA 22217
DR. G. JOINER

PENNSYLVANIA STATE UNIVERSITY
UNIVERSITY PARK, PA 16802
DR. J.S. NISBET
DR. P.R. ROHRBAUGH
DR. L.A. CARPENTER
DR. M. LEE
DR. R. DIVANY
DR. P. BENNETT
DR. F. KLEVANS

PRINCETON UNIVERSITY
PLASMA PHYSICS LABORATORY
PRINCETON, NJ 08540
DR. F. PERKINS

SCIENCE APPLICATIONS, INC.
1150 PROSPECT PLAZA
LA JOLLA, CA 92037
DR. D.A. HAMLIN
DR. L. LINSON
DR. E. FRIEMAN

STANFORD UNIVERSITY
STANFORD, CA 94305
DR. P.M. BANKS

U.S. ARMY ABERDEEN RESEARCH
AND DEVELOPMENT CENTER
BALLISTIC RESEARCH LABORATORY
ABERDEEN, MD
DR. J. HEIMERL

UNIVERSITY OF CALIFORNIA,
BERKELEY
BERKELEY, CA 94720
DR. M. HUDSON

UNIVERSITY OF CALIFORNIA
LOS ALAMOS SCIENTIFIC LABORATORY
J-10, MS-664
LOS ALAMOS, NM 87545
M. PONGRATZ
D. SIMONS
G. BARASCH
L. DUNCAN
P. BERNHARDT

UNIVERSITY OF CALIFORNIA,
LOS ANGELES
405 HILLGARD AVENUE
LOS ANGELES, CA 90024
DR. F.V. CORONITI
DR. C. KENNEL
DR. A.Y. WONG

UNIVERSITY OF MARYLAND
COLLEGE PARK, MD 20740
DR. K. PAPADOPOULOS
DR. E. OTT

UNIVERSITY OF PITTSBURGH
PITTSBURGH, PA 15213
DR. N. ZABUSKY
DR. M. BIONDI
DR. E. OVERMAN

UTAH STATE UNIVERSITY
4TH AND 8TH STREETS
LOGAN, UTAH 84322
DR. R. HARRIS
DR. K. BAKER
DR. R. SCHUNK

E

D

FI

2

D